Plasma-assisted combustion of hydrogen swirling flames: Extension of lean blowout limit and NO_x emissions

Jean-Baptiste Perrin-Terrin, Nicolas Vaysse, Daniel Durox, Ronan Vicquelin, Sébastien Candel, Christophe Laux, Antoine Renaud

Plasma-assisted combustion of hydrogen swirling flames: extension of lean blowout limit and NO_x emissions.

Jean-Baptiste Perrin-Terrin[a], Nicolas Vaysse[a,*], Daniel Durox[a], Ronan Vicquelin[a], Sébastien Candel[a], Christophe O. Laux[a], Antoine Renaud[a]

[a] *Laboratoire EM2C, CNRS, CentraleSupélec, Université Paris-Saclay, 8-10 rue Joliot Curie, Gif-sur-Yvette 91192, France*

Abstract

A key challenge in the use of hydrogen in practical combustors is to stabilize the flame at equivalence ratios close and even below the LBO limit. Plasma-Assisted Combustion (PAC) has been shown to improve the ignition, stabilization, and blowout margins of combustion systems for a great variety of fuels. In this work, Nanosecond Repetitively Pulsed (NRP) discharges are applied to extend the lean blowout limit (LBO) of a partially premixed hydrogen-air combustor atmospheric test rig equipped with a special unit injecting gaseous hydrogen in crossflow into a swirling air stream. The plasma is formed between this injector and an electrode placed in the central recirculation zone. The LBO limit of a 2.2-kW, V-attached flame is extended from 0.220 to 0.177 (20% reduction) using NRP discharges with a plasma power of about 1% of the nominal flame power. Spectroscopic measurements indicate that the plasma operates in the non-equilibrium spark regime: a low ionization degree is observed, and the temperature in the interelectrode gap is moderate (3500 K on average). It is found that plasma discharges increase the OH^* concentration at the flame foot, in the vicinity of the plasma location. Burnt gases analyzed at the outlet of the system indicate that low NO_x concentrations are being produced, even at stoichiometric conditions where the Emission Index reaches its maximum value of 1.1 gNO_x/kgH_2. The application of the NRP discharges increases the NO_x concentration at all equivalence ratios. To minimize the power consumption and the NO_x increase, the NRP discharges are applied with a duty cycle where the plasma is discharged during about half of the time. It is shown that the NO_x concentration scales linearly with the plasma power and thus that NO_x emission induced by the plasma can be mitigated by 60% with this technique while still preserving the LBO extension.

Keywords: Plasma-assisted combustion; Hydrogen swirling flames; Lean blowout; NO_x emissions

Information for Colloquium Chairs and Cochairs, Editors, and Reviewers

1) Novelty and Significance Statement

The novelty of this research lies in the use of plasma discharges in pure hydrogen swirling flames. Extending the lean blow-out limit as well as measuring NO_x emissions of such flames when applying NRP discharges is a novel addition to the existing knowledge in the field of plasma-assisted combustion. It is significant because it provides technological proofs of the capacity to operate hydrogen combustion in very lean conditions. It is apparently the first time that plasma discharges are applied to extend the operability limit of pure hydrogen flames.

2) Author Contributions

- J.-B. P.-T. performed the experiments, processed the data (plasma part) and wrote the paper.
- N.V. performed the experiments, processed the data (combustion part) and wrote the paper.
- D.D. supervised the research, designed the experiments, analyzed the data and edited the paper.
- R.V. supervised the research.
- S.C. supervised the research and edited the paper.
- C.L. supervised the research, analyzed the data, edited the paper and obtained the funding.
- A.R. supervised the research, analyzed the data, edited the paper and obtained the funding.

3) Authors' Preference and Justification for Mode of Presentation at the Symposium

The authors prefer **OPP** presentation at the Symposium, for the following reasons:

- The audience would not need to be familiar with the experiment to comprehend an oral presentation of this standalone work.
- Both hydrogen and plasma-assisted combustion are topical issues, likely to arouse discussion.
- The topic of hydrogen combustion in ultra-lean conditions is key for the future of decarbonized combustion.

1. Introduction

Combustion of renewable hydrogen is a potential solution to decarbonize many industrial sectors requiring high-temperature heating. However, H_2 combustion comes with many new challenges for combustion chambers. The hydrogen/air laminar burning velocity is higher than for conventional fuels, causing flashback issues depending on the injector, and the adiabatic flame temperature is also augmented, indicating a risk for higher NO_x production [1, 2]. The high molecular diffusivity of hydrogen makes it prone to thermo-diffusive instabilities whereas hydrogen enrichment may modify the thermo-acoustic coupling in combustion chambers [3]. Extending the operability domain of hydrogen flames to ultra-lean conditions could be a path to safe combustion. However, the proximity with the extinction limit brings up stability issues.

The flame stability can be improved by the application of plasma in burnt or fresh gases. This technique is called Plasma-Assisted Combustion (PAC). Various methods can be used to generate plasma, and one of the most power-effective is the Nanosecond Repetitively Pulsed (NRP) discharge. These discharges use 1-25 kV amplitude voltage pulses lasting a few nanoseconds and repeated at frequencies of the order of 10-100 kHz. Depending on these parameters, several plasma regimes can be reached with NRP discharges [4, 5]. For PAC applications, a spark regime is preferred due to its hydrodynamic, chemical, and thermal effects that enhance combustion [6].

Many PAC experiments using NRP discharges were conducted during the last two decades showing various combustion enhancements. The ignition delay can be reduced [7], thermo-acoustic instabilities can be controlled and mitigated [8–10] and lean blow-out limits can be extended [11–13]. These effects were observed not only on lab-scale burners but also on semi-industrial scale combustors (70 kW [10], 100 kW [14]). They were also demonstrated on a wide variety of fuels: propane [8], methane [8, 9, 11–13], liquid heptane and dodecane [13], kerosene [15], and ammonia [16].

Regarding hydrogen, plasma-assisted combustion of pure H_2 has focused mostly on the ignition enhancement [17], in supersonic conditions [18], at low pressure (0.2 bar) [19] and at high pressure (1-12 bar) [20]. A recent study also focused on the deflagration to detonation transition using NRP discharges and showed that the plasma accelerates the hydrogen combustion [21]. Despite these promising effects of NRP discharges on H_2/air combustion, to the authors' knowledge no studies have focused on the extension of the lean blow-out limit.

Lean combustion is interesting to reduce the burnt gases temperature, and thus mitigate NO_x emissions. This subject is of particular importance for hydrogen combustion since the H_2 adiabatic flame temperature is, as already mentioned, substantially higher than for conventional fossil fuels at the same equivalence ratio [1]. Exploring ultra-lean conditions is the first step to reducing flame temperature. Among the studies of LBO limit extension using NRP discharges, Lacoste et al. compared the NO_x emissions of a propane/air flame with and without the plasma at different equivalence ratios [22]. When the plasma was applied, they measured an increase in NO_x emissions with the plasma power, a conclusion also mentioned by [10]. More recently, Choe et al. [16] applied NRP discharges in ammonia/air flame and showed that the plasma can reduce by 30% the NO_x levels at the exit of the burner. More surprisingly, they observed a decrease in NO_x when the deposited energy increased. This change in the NO_x emissions trends suggests that the effect of PAC on NO_x emissions highly depends on the fuel.

In this work, NRP discharges are applied in a swirl-stabilized H_2/air burner, the SICCA-H2 configuration. The LBO limit is measured with different NRP parameters and the burnt gases are analyzed at the outlet of the burner. An extension of the LBO limit to ultra-lean conditions is shown with a limited NO_x penalty.

2. Experimental setup

2.1. The SICCA-H2 PAC facility

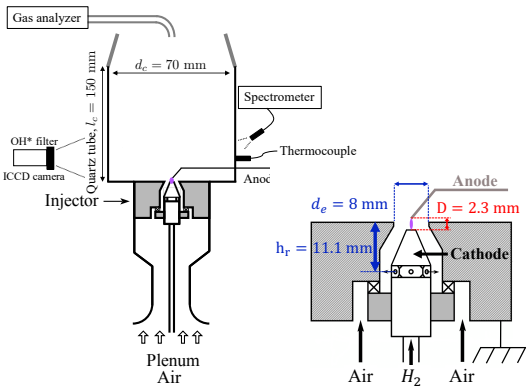

Fig. 1: Left : Schematic view of the SICCA-H2 experimental setup. Right: Schematic view of the CFI-X3 cross-flow injector, equipped with a 1-mm diameter tungsten electrode for NRP discharges.

The experimental configuration is derived from the SICCA-H2 burner presented in [23] which comprises an air plenum, a tangential swirler, a cross-flow injector for gaseous hydrogen (denoted CFI-X) and a cylindrical combustion chamber. In this work, the hydrogen injection head is longer and has a truncated conical shape as presented in Fig. 1. The hydrogen is injected in cross-flow in the swirled air flow through 6 radial holes of 1.2 mm in diameter. In this work, the swirl number is kept constant at a value $S = 0.60$, determined from laser Doppler velocimetry axial and tangential velocity profiles. The quartz

chamber is 150-mm long and surmounted by a 41-mm high 15° converging nozzle that reduces recirculation effects when measuring exhaust gas composition. Air and hydrogen mass flow rates are controlled by two *Bronkhorst* EL-FLOW meters with full-scale capacities of 210 NL/min for air and 20 NL/min for hydrogen and a typical relative accuracy of 0.8%. The hydrogen mass flow rate is kept constant and thus the flame thermal power is fixed at $\mathcal{P}_{th} = 2.2$ kW. The equivalence ratio is varied through the air flow rate while keeping a constant fuel flow rate. Thus, the Reynolds number varies between 8,000 and 36,000.

NRP discharges are applied with a 1-mm diameter tungsten electrode with an end located at $D = 2.3$ mm above the injector tip, in the central recirculation zone. The plasma is formed in this area, between the electrode (anode) and the injector (grounded cathode). Pulses of a fixed duration of 10 ns are generated by an FPG 30-100MC4K pulse generator (FID Technology). The generator is externally triggered by a Pulse-and-Delay BNC model 574, enabling frequency control and time delay adjustment with other devices. The NRP discharges have a positive polarity and their frequency and incident voltage are varied throughout this study in the range 15-30 kHz and 0.5-1.5 mJ.

2.2. Diagnostics

The voltage and the current delivered by the pulses are monitored with voltage (Lecroy PPE20kV) and current (Pearson 6585) probes placed in the middle of the 5-m cables connecting the pulser and the electrode. The time-integration of the product of the voltage by the current gives the energy deposited by each pulse in the interelectrode gap. Then, the product of the frequency by the energy gives the plasma power. More details on these electrical measurements can be found in the appendix of [11]. In the rest of this work, each plasma configuration will be designated by its frequency and the energy deposited per pulse.

The spectra of the flame and the plasma-assisted flame are recorded using an OceanOptics Maya2000Pro deep-UV spectrometer. A Princeton Instruments PI-MAX4 intensified camera equipped with an Asahi Spectra XBPA310 optical bandpass filter centered on 310 nm is used to capture OH^* chemiluminescence images of the flame. The exhaust gas composition is measured using an ECOM J2KN analyzer. The sample probe is placed at the center of the conical exit nozzle, as illustrated in Fig. 1. A non-heated 4-m hose links the sample probe to the gas analyzer.

2.3. Protocol

In this part, the different experimental protocols used in this work are described.

Determination of the equivalence ratio at the LBO limit

A K-type thermocouple placed on the external quartz tube surface measures the wall temperature 30 mm above the backplane. When thermal equilibrium is reached at the combustor wall, the LBO limit is measured by increasing the air flow rate at a rate of 0.1 (NL/min)/s, resulting in an equivalence ratio variation of 0.01 min^{-1}. To detect the blowout two methods are tested. The first consists in recording the time evolution of the air flow rate value and the output signal of a microphone placed at the chamber outlet. The abrupt change in the microphone signal indicates the extinction. Then, the equivalence ratio at the LBO limit is determined via postprocessing of the recorded signals. The second method consists in a direct acoustic detection of the extinction by the experimenter and a direct reading of the air flow value on the controller. Both methods are in good agreement and feature a constant uncertainty of 1% on the air flow rate value at extinction. Thus, the typical uncertainty on the gain in LBO is 4%, computed as a combination of the latter reading uncertainty and statistical uncertainties. In the present work, the results are obtained with the second method.

Measurement of the OH^* chemiluminescence

To measure the OH^* chemiluminescence when the NRP discharges are applied, the camera is externally triggered by the BNC generator to adjust the time delay with the plasma emission. For the non-assisted flame, the camera is internally triggered.

Application of the NRP discharges

In this work, NRP discharges are applied in two modes:

- The continuous mode, which is the most commonly used in the literature.
- The duty-cycle mode, used in [14, 24].

The pulsing pattern of the duty-cycle mode is described in Fig. 2. This mode consists in repetitively applying bursts of NRP discharges. At a given frequency, the duty-cycle is described by the number of pulses ON in the burst (N_{ON}) and the number of following pulses OFF (N_{OFF}). In Fig. 2, $N_{\text{ON}} = 6$ and $N_{\text{OFF}} = 5$. The duty-cycle ratio is defined as $r_{\text{DC}} = N_{\text{ON}}/(N_{\text{ON}} + N_{\text{OFF}})$ and corresponds to the fraction of the cycle during which the plasma is on. The continuous mode corresponds to the limit case where $r_{\text{DC}} = 1$. In the duty-cycle mode, the plasma power is $P_{\text{plasma}} = f \times E_p \times r_{\text{DC}}$. Thus, the lower the duty-cycle ratio, the lower the plasma power.

Burnt gases analysis

After each variation of the experimental conditions, a few minutes are necessary for the measured dry concentration to stabilize. Once stabilized, their values are noted. The analysis of the dry gases composition gives, among others, the dry mole fractions of O_2,

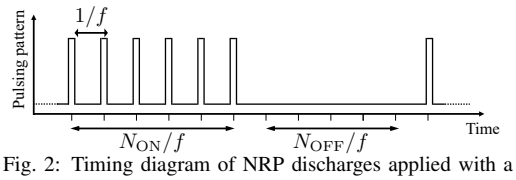

Fig. 2: Timing diagram of NRP discharges applied with a duty-cycle, here with $N_{\mathrm{ON}} = 6$ and $N_{\mathrm{OFF}} = 5$.

NO, NO_2 and H_2. Because the unburnt H_2 rapidly saturates the ECOM analyzer (the mole fraction limit is 23000 ppm), H_2 cannot be measured when the combustion efficiency is not close to unity. The following global chemical equation is used for the post-processing of the dry mole fractions:

$$\phi\,\mathrm{H_2} + \frac{1}{2}\left(\mathrm{O_2} + \beta\,\mathrm{N_2}\right) \rightarrow$$
$$\eta\phi\,\mathrm{H_2O} + \frac{1-\eta\phi}{2}\,\mathrm{O_2} + \frac{\beta}{2}\,\mathrm{N_2} + \phi(1-\eta)\,\mathrm{H_2}$$

where $\beta = n'_{N_2}/n'_{O_2} = 3.76$ is the nitrogen-to-oxygen ratio in fresh air and $\eta = n''_{H_2O}/n'_{H_2}$ is the combustion efficiency. The number of moles n'_i and n''_i respectively stand for the reactants and the products of species i. The mole fraction of oxygen under dry conditions can be expressed as:

$$X^m_{O_2} = \frac{n''_{O_2}}{n''_{O_2} + n''_{N_2} + n''_{H_2}} = \frac{1-\eta\phi}{1+\beta+(2-3\eta)\phi}$$

thus the combustion efficiency can be deduced from $X^m_{O_2}$ and the global equivalence ratio ϕ:

$$\eta\phi = \frac{(\beta+1+2\phi)X^m_{O_2} - 1}{3X^m_{O_2} - 1}$$

One retrieves the limit case of no combustion, for which $X^m_{O_2} = 1/(1+2\phi+\beta)$ leads to $\eta = 0$, and the case of complete combustion where $X^m_{O_2} = (1-\phi)/(1-\phi+\beta)$ leads to $\eta = 1$.

One can then derive the wet mole fractions by multiplying the measured dry mole fractions by a dry-to-wet correction factor C, defined as:

$$C = \frac{n''_{O_2} + n''_{N_2} + n''_{H_2}}{n''_{H_2O} + n''_{O_2} + n''_{N_2} + n''_{H_2}}$$

After some algebra one finds that:

$$C = \frac{\phi + \beta/2 - 1}{\phi + \beta/2 - X^m_{O_2}(1+\beta+2\phi)}$$

which gives, in the limit case of no combustion, $C = 1$ which is consistent with the fact that no water is produced. In the complete combustion assumption, one retrieves the classical formula $C = (\beta+1-\phi)/(\beta+1+\phi)$.

The evolution of C is shown in Fig. 3.

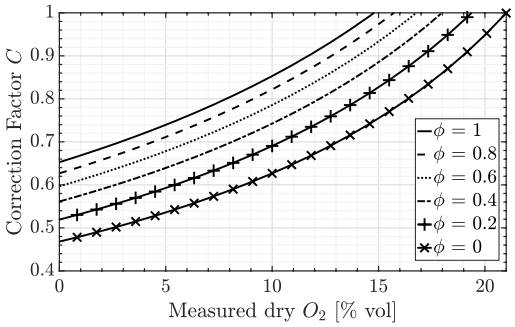

Fig. 3: Abacus giving the correction factor C linking dry and wet mole fractions, as a function of the measured O_2 dry mole fraction and the equivalence ratio.

Electrode erosion

Electrode erosion was observed both when operating the flame with and without plasma. The erosion speed was about 0.5 mm/h with the flame alone and 0.6 mm/h with the flame and plasma at 40 kHz and 1.5 mJ. For this reason, the electrodes were replaced after each hour of operation to prevent a variation of more than 0.6 mm in the interelectrode gap distance during experiments. Additionally, to minimize this uncertainty for each operating point, several electrodes with different erosion states are used.

3. Experimental conditions

3.1. Flame structure

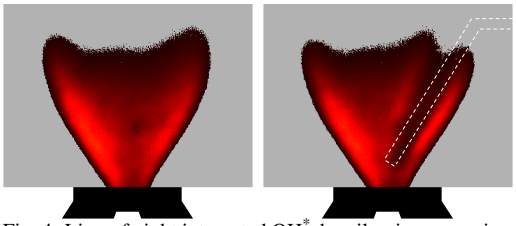
Fig. 4: Line-of-sight integrated OH^* chemiluminescence images of the flame without plasma, at thermal power $\mathcal{P}_{th} = 2.2$ kW and equivalence ratio $\phi = 0.231$, (left) without and (right) with the electrode outlined with white dashes.

The observed LBO equivalence ratio of the flame at thermal power $\mathcal{P}_{th} = 2.2$ kW is $\phi = 0.220$. At $\phi = 0.231$, corresponding to 105% of the LBO limit, the flame is V-shaped and is attached to the injector flat tip. The OH^* chemiluminescence images of Fig. 4 show that the presence of the electrode brings minimal changes to the flame shape (the electrode can be seen in the right image of Fig. 4).

3.2. Characterization of the plasma

NRP discharges are generated with frequencies in the range of 15 – 30 kHz and with incident voltages

in the range of 1.5 – 3 kV. The typical shapes of the voltage and current traces are shown in Fig. 5. The interelectrode distance is $D = 2.3 \pm 0.6$ mm. The energy is deposited during the initial pulse and the series of reflected pulses (as shown in blue in Fig. 5) and varies between 0.5 mJ and 1.5 mJ, with an uncertainty of ± 100 µJ. In these conditions, according to [4], the plasma is formed in the spark regime.

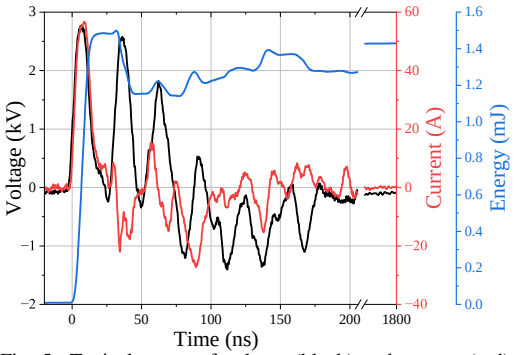

Fig. 5: Typical traces of voltage (black) and current (red) of a pulsed discharge. The energy (blue) is the integration over time of the product of the voltage by the current. In this case, the incident voltage is 2.8 kV, and the deposited energy is 1.42 mJ after 1800 ns.

The optical emission spectroscopy measurements shown in Fig. 6 are used to measure the temperature in the plasma region from the rotational temperature of $N_2(C)$ in the range 360 – 390 nm using Specair [25]. A temperature of 3500 $\pm$ 300 K is found for the 15 kHz – 1.5 mJ plasma (applied continuously and with duty-cycle) and 3800 $\pm$ 400 K for the 30 kHz – 0.75 mJ plasma. Additionally, an upper bound of the electron number density can be estimated from the broadening of the H_β line at 486 nm [26]. The total broadening observed in Fig. 6 is 1.5 nm. Taking into account the instrumental broadening of about 1 nm, we obtain an upper bound of the ionization degree of less than about 0.2%. Considering the relatively low heating and ionization degree, the plasma is in the non-equilibrium spark regime [5].

The spectrum of the flame without plasma is dominated by the black-body emission of the heated electrode. In particular, the broadband blue emission characteristic of the hydrogen flames is not visible. The absorption caused by the water vapor produced by the combustion appears around 950 nm. At 310 nm, OH^* emission is not intense because the field of view of the spectrometer is centered on the discharge which produces intense emission via the second positive system of nitrogen.

4. Results

4.1. Influence of frequency and deposited energy per pulse on LBO extension

In a first set of experiments, the frequency is kept equal to 30 kHz and the deposited energy per pulse varies with values 500 µJ, 750 µJ, 1 mJ, and 1.5 mJ. Fig. 7 shows that the gain in LBO compared to the non-assisted case increases linearly with the energy, with values of 6%, 11%, 19%, and 23%. Then, measurements are performed at a lower frequency, $f = 15$ kHz, and show that the gain in LBO also increases with the frequency at $E_p = 0.75$ mJ (from 7% to 11%) and $E_p = 1.5$ mJ (from 20% to 23%). It is interesting to compare in Fig. 7 two experiments with the same average plasma power. The $f = 15$ kHz - $E_p = 1.5$ mJ and the $f = 30$ kHz - E_p = 0.75 mJ plasmas are on the 22.5-W line (corresponding to 1% of the flame thermal power) but it is shown in Table 1 that the former extends the LBO limit by up to 19.5% while the latter only to 10.9%. This indicates that in these conditions, increasing the energy extends the LBO limit more efficiently than increasing the repetition frequency at constant plasma power. Because of its larger improvement in LBO limit, the $f = 15$ kHz - $E_p = 1.5$ mJ plasma will be studied in more detail in the rest of this work.

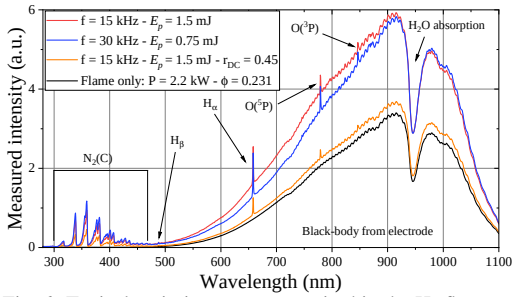

Fig. 6: Typical emission spectra acquired in the H_2 flame at $\mathcal{P}_{th} = 2.2$ kW and $\phi = 0.231$. Spectra are acquired during 50 ms and averaged 40 times. The black line is acquired without the plasma. The red and orange lines are acquired with the 15 kHz – 1.5 mJ plasma, applied respectively continuously and with a duty-cycle ratio of 0.45. The blue line is acquired with the 30 kHz - 0.75 mJ plasma applied continuously.

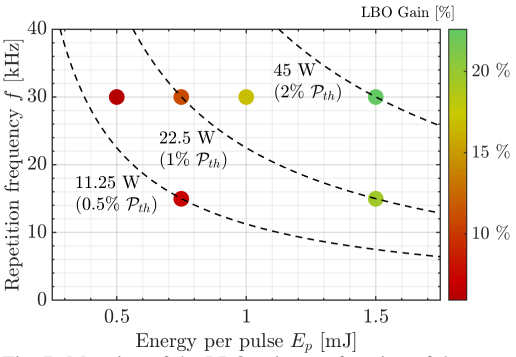

Fig. 7: Mapping of the LBO gain as a function of the repetition frequency and the average energy deposited per pulse. Dashed lines represent isolines of plasma power, expressed as a percentage of the thermal power.

Table 1: LBO measurements for a flame at $\mathcal{P}_{th} = 2.2$ kW

Frequency [kHz]	-	15	15	30	30
Energy [mJ]	-	0.75	1.5	0.75	1.5
ϕ at LBO	0.220	0.204	0.177	0.196	0.170
Gain in LBO [%]	0	7.3	19.5	10.9	22.6
Plasma power [W]	0	11.25	22.5	22.5	45

The effect of the plasma pulses on the chemistry of the flame is analyzed through phase-averaged OH^* chemiluminescence imaging presented in Fig. 8. The images are recorded during the time separating two pulses and show that the plasma locally increases the OH^* radical concentration near the foot of the flame front, where it is applied. Right after the discharge, the OH^* signal is intense in the vicinity of the electrode. Then, the intensity monotonically decreases until the following pulse. This effect is emphasized in the bottom row of Fig. 8, which isolates the contribution of plasma to the OH^* signal by subtracting the OH^* image of the flame without plasma shown in Fig. 4 from the phase-averaged images. It also highlights that the effect of the plasma on the flame is local and does not increase the OH^* chemiluminescence elsewhere in the flame.

4.2. Combustion efficiency

The values of the combustion efficiency presented in Fig. 9 include the flame without plasma and the plasma-assisted flame in the three investigated plasma cases: $f = 15$ kHz - $E_p = 1.5$ mJ, $f = 30$ kHz - $E_p = 0.75$ mJ and $f = 15$ kHz - $E_p = 1.5$ mJ applied with a duty-cycle ratio $r_{\rm DC} = 0.45$. At first, the combustion efficiency increases with the equivalence ratio. Then, a plateau value of $92\% \pm 8\%$ is reached above $\phi = 0.5$. However, the measured mole fraction of H_2 is 0 ppm in this domain, indicating that combustion is complete. In stoichiometric conditions, the efficiency is close to 100%. No clear effect of the plasma on the combustion efficiency of the flame is visible in Fig. 9.

4.3. NO_x emissions

The measured dry NO_x mole fractions are multiplied by the dry-to-wet correction factor C introduced in Fig. 3 to obtain their wet values in the flame. This is essential to derive an emission index based on the mass flow rate ratio between NO_x and injected H_2. The evolution of this NO_x Emission Index, plotted in Fig. 10, shows that the NO_x emissions of the non-assisted flame remain lower than 1.1 g/kgH_2 on the whole investigated operability domain of the flame. This value corresponds to the lower end of the typical Emission Indexes reported in the literature (1-20 g/kgH_2 for jet and coaxial flames [27–29]). The NO_x emissions increase with the equivalence ratio after a slight decrease in the leanest range. An optimum for NO_x emissions is found around $\phi = 0.4$ for all conditions. All plasma pulses investigated in this work induce an increase of the NO_x emissions by 0.5 to 1.5 g/kgH_2. However, applying a duty-cycle (green diamonds in Fig. 10) to the $f = 15$ kHz - E_p =1.5 mJ plasma reduces the NO_x emissions at all equivalence ratios, up to 60% in the leanest domain, while still extending the LBO limit. The one-sigma error bars are fairly large because all sources of error are taken into account. The main uncertainties arise when the oxygen mole fraction is close to zero near stoichiometry or at very low equivalence ratios (especially in Fig. 10). However, the measured mean values still clearly support the reduction of NO_x emissions in duty cycle mode, which is the intended point of Fig. 10. The effect of this technique on the NO_x emissions is further investigated in the following section.

4.4. Influence of the pulsing pattern : effect of the duty-cycle on flame stability and NO_x emissions

To decrease the plasma power without reducing the effect of the plasma on the flame, the NRP discharges are applied in the duty-cycle mode at $f = 15$ kHz and $E_p = 1.5$ mJ. This method was already tested by [14, 24] and the energy was reduced without losing the stabilizing properties of the plasma. The power consumption is thus directly multiplied by $r_{\rm DC}$. The equivalence ratio is fixed at 105% of the LBO limit obtained with this plasma ($1.05\phi^p_{LBO} = 0.186$). To determine the lowest duty-cycle ratio allowing the stabilization of a flame at this equivalence ratio, $N_{\rm ON}$ is fixed and $N_{\rm OFF}$ is progressively increased until the flame is blown off. The gas is sampled in the process. The results are shown in Fig. 11. The extinction limit is drawn as a dotted line and presents the same V-shape as found in [14], with a minimum reached around $N_{\rm ON} = 100$. During the ON phase, the pulses generate a stabilizing kernel, enhancing the combustion. During the OFF phase, the enhancement of the flame fades until the next ON phase. For the low $N_{\rm ON}$, the aforementioned combustion-stabilizing kernel is not strong enough and the enhancement fades before the next ON phase. When $N_{\rm ON}$ increases, the kernel is stronger, and thus the maximum $r_{\rm DC}$ is larger. As $N_{\rm ON}$ is further increased, for a given $r_{\rm DC}$, the OFF phase is also longer and the contribution of the additional pulses to the kernel is not sufficient to sustain the combustion on this longer OFF phase: the flame extinguishes.

Two key plasma-induced reactions must be considered to interpret the results on NO_x emissions presented in Fig. 11: the beneficial radical production (1) and the detrimental NO formation (2).

$$N_2^* + O_2 \rightarrow N_2 + 2\,O \quad (1)$$

$$N_2^* + O \rightarrow NO + N \quad (2)$$

where N_2^* stands for excited electronic states of nitrogen. The flame is stabilized when successive pulses have produced enough radicals through reaction (1).

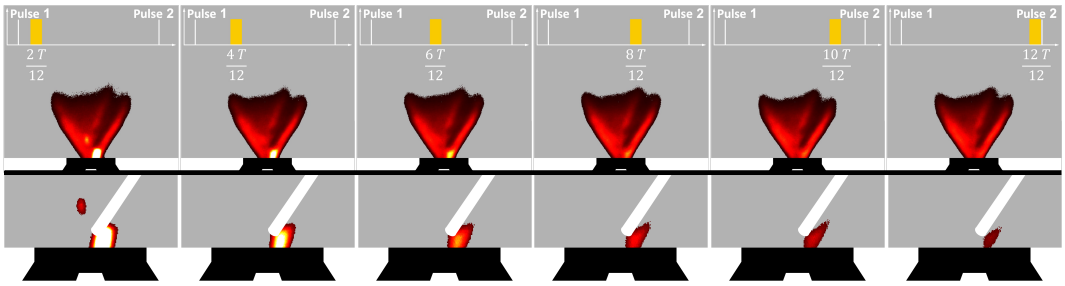

Fig. 8: Phase-averaged OH* chemiluminescence images of the flame between two plasma pulses. The phase number is indicated in the top diagram. The $f = 15$ kHz - $E_p = 1.5$ mJ plasma is applied. Top: line-of-sight integrated images of the flame. Bottom: Images of the difference between these phase-averaged images and the image of the flame without plasma, presented in Fig. 4. The electrode is added in white on the second row. The exposure time is 5 µs. Twelve phases are recorded, only the even phases are shown.

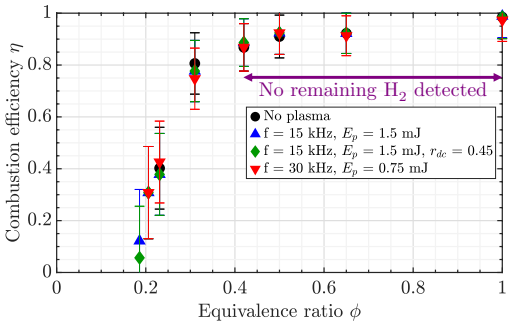

Fig. 9: Evolution of the combustion efficiency as a function of the equivalence ratio, for the flame without plasma, and the three different discharges applied. The efficiency is computed from the dry O_2 mole fraction measurement and the equivalence ratio. Uncertainties are propagated starting from the accuracy and resolution of the mass flow meters and the gas analyzer.

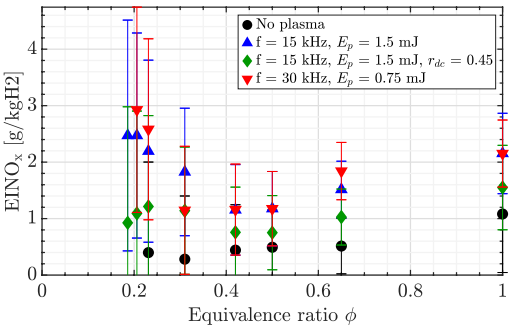

Fig. 10: Evolution of the NO_x Emission Index as a function of the equivalence ratio, for the flame without plasma, and for the three different discharges applied. The $EINO_x$ is computed from the dry NO_x mole fractions, corrected to wet conditions using O_2 measurements. Uncertainties are propagated starting from the accuracy and resolution of the mass flow meters and the gas analyzer.

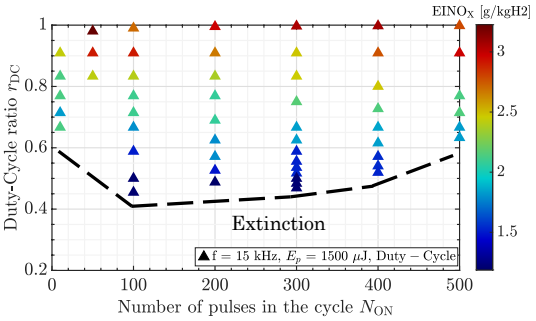

Fig. 11: Map of the NO_x Emission Index as a function of the duty-cycle ratio r_{DC} and the number of pulses in each cycle, at an equivalence ratio of $1.05\phi^p_{LBO} = 0.186$. The $f = 15$ kHz - $E_p = 1.5$ mJ plasma is applied. The dashed line shows the minimal duty-cycle ratio required to stabilize the flame.

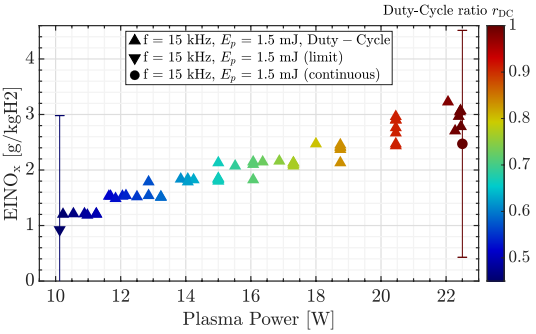

Fig. 12: Evolution of the NO_x Emission Index as a function of the plasma power at an equivalence ratio of $1.05\phi^p_{LBO} = 0.186$. The $f = 15$ kHz - $E_p = 1.5$ mJ plasma is applied. The colors correspond to the duty-cycle ratio. The down triangle corresponds to the measured emissions at the minimal r_{DC} value and the circle to the value obtained for continuous plasma operation. N_{ON} is varied between 10 and 500.

Above this threshold, additional pulses do not further improve stabilization, but they increase NO through reaction (2). Thus, the duty cycle mode allows to keep the same LBO while minimizing the NO_x penalty.

The effect of the pulsing pattern on NO_x emissions is expressed in Fig. 12 as a function of the average plasma power, computed as the product of the duty-cycle ratio with the continuous plasma power. The NO_x emissions decrease linearly with

the plasma power as the duty-cycle ratio is decreased. This is consistent with the results found in methane flames [10, 14, 22].

5. Conclusion

A V-attached hydrogen flame of 2.2 kW is studied. Its equivalence ratio at the lean blow-out limit equals 0.22. NRP discharges are applied to this flame to extend the LBO limit. Various couples of repetition frequencies and deposited energy are tested. In all NRP conditions, the plasma is in the non-equilibrium spark regime, inducing moderate heating (a few thousand kelvins) and a low ionization degree (less than 0.2%). The effect of the plasma on the flame is observed using OH^* chemiluminescence. During the pulse, the plasma locally increases the OH^* signal. The increase is confined to the vicinity of the plasma and slowly decays between two pulses. The main findings of this work are:

- The LBO limit can be extended from 0.22 to 0.177 (20% gain) with the $f = 15$ kHz - E_p =1.5 mJ plasma.
- The plasma power required to extend the LBO limit with continuously applied NRP discharges is about 1% of the flame thermal power.
- The plasma power can be reduced to 0.45% of the flame thermal power by applying the NRP discharges with a duty-cycle ratio of 0.45.
- From $\phi = 0.22$ to 1 (lean operation) the non-assisted flame emits less than 1.1 gNO_x/kgH_2.
- The NRP discharges applied continuously increase the NO_x emission by 0.5 to 1.5 g/kgH_2.
- The NRP discharges applied with a duty-cycle ratio of 0.45 increase the NO_x emission by 0.2 to 0.9 g/kgH_2.

Declaration of competing interest

The authors declare that they have no known competing financial interests or personal relationships that could have appeared to influence this work.

Acknowledgments

This work was partially supported by the FlyHy project of the Agence Nationale de la Recherche (ANR-21-CE05-0008), the European Research Council (ERC) under the European Union's Horizon 2020 research and innovation program (GreenBlue project under grant agreement No.101021538) and by the Fondation Simone and Cino Del Duca through a scientific grant attributed to the project PLATHON. For open access purposes, a CC-BY license has been applied by the authors to this document and will be applied to any subsequent version up to the author's manuscript accepted for publication resulting from this submission. The authors would like to thank Yannick Le Teno and the support team of EM2C lab for their technical assistance.

References

[1] A. L. Sánchez, F. A. Williams, Recent advances in understanding of flammability characteristics of hydrogen, Progress in Energy and Combustion Science 41 (2014) 1–55.

[2] P. Palies, Challenges and Outlook for Hydrogen-Based Aviation, AIAA Paper 2022-3378. (2022) 15.

[3] J. G. Aguilar, E. Æsøy, J. R. Dawson, The influence of hydrogen on the stability of a perfectly premixed combustor, Combustion and Flame 245 (112323) (Nov. 2022).

[4] D. Z. Pai, D. A. Lacoste, C. O. Laux, Transitions between corona, glow, and spark regimes of nanosecond repetitively pulsed discharges in air at atmospheric pressure, Journal of Applied Physics 107 (9) (2010) 093303.

[5] N. Minesi, S. Stepanyan, P. Mariotto, G. D. Stancu, C. O. Laux, Fully ionized nanosecond discharges in air: The thermal spark, Plasma Sources Science and Technology 29 (8) (2020) 085003.

[6] C. Laux, Applications of Plasma Discharges to Combustion, Journal of the Combustion Society of Japan 64 (209) (2022) 257–264.

[7] Y. Xiong, O. Schulz, C. Bourquard, M. Weilenmann, N. Noiray, Plasma enhanced auto-ignition in a sequential combustor, Proceedings of the Combustion Institute 37 (4) (2019) 5587–5594.

[8] J. Moeck, D. Lacoste, C. Laux, C. Paschereit, Control of combustion dynamics in a swirl-stabilized combustor with nanosecond repetitively pulsed discharges, in: 51st AIAA Aerospace Sciences Meeting Including the New Horizons Forum and Aerospace Exposition, Aerospace Sciences Meetings, 2013.

[9] L. Yu, B. Aravind, D. A. Lacoste, Mitigating the response of premixed swirl flames to acoustic excitation by nanosecond repetitively pulsed discharges at elevated pressures, Combustion and Flame 256 (2023) 112944.

[10] B. Dharmaputra, S. Shcherbanev, B. Schuermans, N. Noiray, Thermoacoustic stabilization of a sequential combustor with ultra-low-power nanosecond repetitively pulsed discharges, Combustion and Flame 258 (2023) 113101.

[11] N. Q. Minesi, V. P. Blanchard, E. Pannier, G. D. Stancu, C. O. Laux, Plasma-assisted combustion with nanosecond discharges. I: Discharge effects characterization in the burnt gases of a lean flame, Plasma Sources Science and Technology 31 (4) (2022) 045029.

[12] F. Di Sabatino, D. A. Lacoste, Enhancement of the lean stability and blow-off limits of methane-air swirl flames at elevated pressures by nanosecond repetitively pulsed discharges, Journal of Physics D: Applied Physics 53 (35) (2020) 355201.

[13] G. Vignat, N. Minesi, P. R. Soundararajan, D. Durox, A. Renaud, V. Blanchard, C. O. Laux, S. Candel, Improvement of lean blow out performance of spray and premixed swirled flames using nanosecond repetitively pulsed discharges, Proceedings of the Combustion Institute 38 (4) (2021) 6559–6566.

[14] V. P. Blanchard, P. Scouflaire, C. O. Laux, S. Ducruix, Combustion performance of plasma-stabilized lean flames in a gas turbine model combustor, Applications in Energy and Combustion Science 15 (2023) 100158.

[15] G. Heid, G. Pilla, R. Lecourt, D. Lacoste, Assisted Combustion Of An Air Kerosene Mixture By Nanosecond Repetitively Pulsed Discharges, in: Inter-

national Symposium on Air Breathing Engines, American Institute of Aeronautics and Astronautics, Montreal, Canada, 2009, pp. 474–482.
[16] J. Choe, W. Sun, T. Ombrello, C. Carter, Plasma assisted ammonia combustion: Simultaneous NOx reduction and flame enhancement, Combustion and Flame 228 (2021) 430–432.
[17] Y. Ju, X. Mao, J. K. Lefkowitz, H. Zhong, Plasma-Assisted Hydrogen Combustion, in: E.-A. Tingas (Ed.), Hydrogen for Future Thermal Engines, Green Energy and Technology, Springer International Publishing, Cham, 2023, pp. 429–458.
[18] H. Do, M. A. Cappelli, M. G. Mungal, Plasma assisted cavity flame ignition in supersonic flows, Combustion and Flame 157 (9) (2010) 1783–1794.
[19] A. Dutta, Z. Yin, I. V. Adamovich, Cavity ignition and flameholding of ethylene–air and hydrogen–air flows by a repetitively pulsed nanosecond discharge, Combustion and Flame 158 (8) (2011) 1564–1576.
[20] S. A. Shcherbanev, N. A. Popov, S. M. Starikovskaia, Ignition of high pressure lean H2:air mixtures along the multiple channels of nanosecond surface discharge, Combustion and Flame 176 (2017) 272–284.
[21] J. A. T. Gray, D. A. Lacoste, Effect of the plasma location on the deflagration-to-detonation transition of a hydrogen–air flame enhanced by nanosecond repetitively pulsed discharges, Proceedings of the Combustion Institute 38 (3) (2021) 3463–3472.
[22] D. A. Lacoste, J. P. Moeck, C. O. Paschereit, C. O. Laux, Effect of Plasma Discharges on Nitric Oxide Emissions in a Premixed Flame, Journal of Propulsion and Power 29 (3) (2013) 748–751.
[23] N. Vaysse, D. Durox, R. Vicquelin, S. Candel, A. Renaud, Stabilization and Dynamics of Pure Hydrogen Swirling Flames Using Cross-Flow Injection, in: ASME Turbo Expo 2023: Turbomachinery Technical Conference and Exposition, American Society of Mechanical Engineers Digital Collection, 2023.
[24] A. M. Alkhalifa, A. Alsalem, D. Del Cont-Bernard, D. A. Lacoste, Active control of thermoacoustic fluctuations by nanosecond repetitively pulsed glow discharges, Proceedings of the Combustion Institute 39 (4) (2023) 5429–5437.
[25] C. O. Laux, T. G. Spence, C. H. Kruger, R. N. Zare, Optical diagnostics of atmospheric pressure air plasmas, Plasma Sources Science and Technology 12 (2) (2003) 125.
[26] N. Konjević, M. Ivković, N. Sakan, Hydrogen Balmer lines for low electron number density plasma diagnostics, Spectrochimica Acta Part B: Atomic Spectroscopy 76 (2012) 16–26.
[27] J. F. Driscoll, R.-H. Chen, Y. Yoon, Nitric oxide levels of turbulent jet diffusion flames: Effects of residence time and damkohler number, Combustion and Flame 88 (1) (1992) 37–49.
[28] S. Noda, J. Inohae, Z. S. Saldi, NO emission characteristics of confined jet nonpremixed flames, Proceedings of the Combustion Institute 31 (1) (2007) 1625–1632.
[29] M. Leroy, C. Mirat, A. Renaud, S. Puggelli, S. Zurbach, R. Vicquelin, Structure and NOx Emissions of Stratified Hydrogen-Air Flames Stabilized on a Coaxial Injector, Journal of Engineering for Gas Turbines and Power 146 (031012) (Nov. 2023).